Fiber Parameter Identification and Monitoring Using a Koopman-Based Identification Method

Aamir, Shahzeb; Wahls, Sander

DOI
10.1109/JLT.2025.3546172

Publication date
2025

Document Version
Final published version

Published in
Journal of Lightwave Technology

Fiber Parameter Identification and Monitoring Using a Koopman-Based Identification Method

Shahzeb Aamir and Sander Wahls, *Senior Member, IEEE*

***Abstract*—Knowledge of fiber parameters is paramount for efficient fiber optic communication. We investigate the suitability of a recently proposed Koopman operator-based parameter estimation method for partial differential equations for the identification of single-span fiber links of various lengths in simulations. The Koopman-based identification method does not require spatial derivatives, which makes it especially suitable for the estimation of fiber parameters. The method also does not require specific training signals or devices. It can estimate the parameters using transmitted and received signals from an operational link. We identify the dispersion length as a critical parameter for the accuracy of the method and show that it can jointly identify the fiber parameters at optimal transmit powers for four different fiber types, with the worst relative error below 20% in identifying the Kerr parameter. The loss and dispersion coefficients are identified more accurately in all the scenarios considered with relative errors below 5%. We also compare the algorithm against other fiber parameter estimation techniques, such as conserved quantity identification and direct identification (based on discretization of the spatiotemporal domain). We finally demonstrate that the algorithm detects changes in the fiber parameters more accurately than the parameters themselves, which can be exploited for link monitoring.**

***Index Terms*—Fiber optics, identification, Koopman operator, PDEs.**

I. Introduction

THE efficient transmission of data in optical fiber links requires knowledge of fiber parameters such as the loss, dispersion and Kerr nonlinearity coefficients. Fiber manufacturers provide these parameters on the datasheets for their fibers, which have been measured under lab conditions. However, fiber parameters can change during operation due to aging, bending, temperature changes, etc. The growing mismatch between the assumed and true fiber parameters can have a negative impact on transmission quality. The changing (or changed) fiber parameters can also point towards an imminent (or current) link failure. We therefore consider the problem of reestimating the fiber parameters of an operational link, where we assume that input-output data from the link is available (i.e. transmitted and corresponding received signals), but that the inputs cannot be chosen freely. This rules out methods that require special hardware or specific probing signals [3]. We remark that it is possible to work with output data only, if the input data can be reconstructed from the decoded bits.

One possible approach to tackle the fiber parameter estimation would be to use conventional partial differential equation (PDE) parameter estimation methods, e.g., based on a linear equation system obtained from discretizing temporal and spatial derivatives [4], [5]. The disadvantage of these methods is that derivatives need to be estimated in both space and time. For fibers, where only inputs and outputs are measured, estimating spatial derivatives is not possible for longer span lengths. Recently, a novel identification method for the dispersion and Kerr coefficients based on nonlinear Fourier transforms (NFT) [6], [7] was proposed. The advantage of this method is that no spatial derivatives have to be found. However, like all NFT methods, this method relies on a path-average approximation when applied to standard single mode fiber (SSMF), which introduces additional errors. This is because only the lossless nonlinear Schrödinger equation is solved exactly by the NFT. Furthermore, the loss coefficient has to be known a priori. A conceptually related approach is to exploit conserved quantities [6]. Yet another approach to identify the fiber parameters is to propagate the input data numerically, e.g. using a Fourier split-step method, for different candidate fiber parameters, e.g. chosen from grids, and to keep the parameters for which the numerical output matches true output best [7]. This approach is simple and reliable, but the computational complexity suffers from the curse of dimensionality as the number of parameters increases. It is therefore ideally used to identify the Kerr coefficient when the other coefficients are already known. For such scenarios, there are also adaptive digital backpropagation methods to estimate the Kerr coefficient [8], [9]. Recently, the physics-informed neural network (PINN) approach [10] was also used to estimate fiber parameters. The method performs well in estimating the fiber parameters. However, it comes with the difficulty of tuning the hyperparameters of the neural network. Moreover, it only considers simple on-off keying (OOK) transmitted signals. It is not clear if the PINN approach can handle more complex transmitted signals. Re-tuning PINNs for different scenarios can also present a computational overhead.

In this paper, we are interested in methods that estimate all fiber parameters jointly and with a low computational

Received 27 September 2024; revised 31 January 2025; accepted 19 February 2025. Date of publication 26 February 2025; date of current version 2 June 2025. *(Corresponding author: Shahzeb Aamir.)*

Shahzeb Aamir is with the Delft Center for System and Control, Delft University of Technology, 2628 CD Delft, The Netherlands (e-mail: s.aamir@tudelft.nl).

Sander Wahls is with the Karlsruhe Institute of Technology, Institute of Industrial Information Technology, 10587 Berlin, Germany (e-mail: sander.wahls@kit.edu).

This article has supplementary material provided by the authors and color versions of one or more figures available at https://doi.org/10.1109/JLT.2025.3546172.

Digital Object Identifier 10.1109/JLT.2025.3546172

complexity. Therefore, we investigate the performance of a recently proposed PDE parameter estimation technique [11] (based on [12]) that exploits the Koopman operator framework. Koopman operators, originally introduced in [13], have recently obtained much attention as a tool to linearize nonlinear systems *globally*. This is in contrast to conventional *local* linearization. The Koopman operator thereby provides new observables under which the evolution of the system becomes linear. See, e.g., [14], [15] for introductions to the topic. The method in [11] seems attractive for fiber identification because it is simple and does not require spatial derivatives. While it is known that the span length cannot be arbitrarily large, the current theory cannot tell us for which span lengths the performance will still be acceptable.

In this study, our goal is thus to assess the suitability of the Koopman-based identification method (KIM) for optical fiber transmission scenarios. We evaluate the performance of the proposed method for various fiber types on single span links with an Erbium Doped Fiber Amplifier (EDFA) by considering single- and dual-polarized signals governed by the nonlinear Schrödinger equation (NLSE) and Manakov equations, respectively. Currently, we have not extended evaluation to multiple span links. Moreover, we also consider the problem of tracking changes in the fiber parameters in an operational single-span link using KIM. Our main contributions are as follows.

- The KIM is shown to work well for fiber links up to 60 km in extensive simulations of four different fiber types.
- The dispersion length $T^2/|\beta_2|$ is identified as the critical factor influencing the accuracy of KIM.
- The KIM is extended to vector-valued signals so that it applies to dual-polarization transmissions.
- It is demonstrated that a large part of the bias in KIM estimates for longer links cancels out when considering changes in the parameters. This makes the method especially suitable for link monitoring.

The paper is organized as follows. The fiber model is explained in Section II. The Koopman-based identification method is first explained in Section III. The simulation setup is then detailed in Section IV. The results regarding the direct parameter estimation using the KIM are presented and discussed in Section V. Section VI presents the results for a link monitoring scenario, where changes in the fiber parameters are tracked using the KIM. The paper concludes in Section VII.

II. Fiber Models

The nonlinear Schrödinger equation governs the propagation of light through a single-mode optical fiber link under the influence of attenuation, anomalous dispersion, and self-focusing [16]:

$$u_z = -\frac{\alpha}{2}u - i\frac{\beta_2}{2T_0^2}u_{\tau\tau} + i\gamma|u|^2u, \tag{1}$$

where $u(\tau, z)$ is the complex field envelope, τ and z are normalized retarded time and location in the fiber, respectively. Furthermore, $i = \sqrt{-1}$ and T_0 is a normalization constant that arises when normalizing the retarded time, i.e., $\tau = t/T_0$. The loss, dispersion, and Kerr nonlinearity coefficients are denoted by α, β_2, and γ, respectively. The subscripts $_z$ and $_\tau$ indicate partial derivatives.

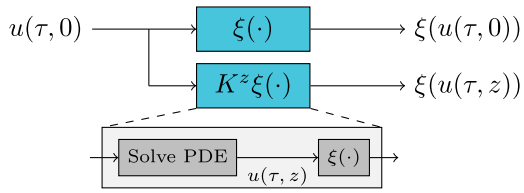

Fig. 1. The effect of the Koopman operator K^z on an observable ξ.

Additive white Gaussian noise is also taken into account, which enters the system because of EDFA located at the end of the fiber. The noise power is dependent on the noise figure of EDFA, fiber span length (denoted by Z), and loss coefficient.

We also consider Manakov equations, which governs the propagation of dual polarized light in a single mode optical fiber link [17]:

$$\begin{cases} u_z = -\frac{\alpha}{2}u - i\frac{\beta_2}{2T_0^2}u_{\tau\tau} + i\frac{8}{9}\gamma(|u|^2 + |v|^2)u, \\ v_z = -\frac{\alpha}{2}v - i\frac{\beta_2}{2T_0^2}v_{\tau\tau} + i\frac{8}{9}\gamma(|v|^2 + |u|^2)v, \end{cases} \tag{2}$$

where u and v are the complex field envelopes of two polarizations. The rest of the notations are similar to the one given in (1). We consider these two fiber models to test the suitability of the Koopman-based identification method.

III. Koopman-Based Identification Method (KIM)

A. Primer on Koopman Operator Theory

Before describing the Koopman-based identification algorithm, we introduce Koopman operators and their semigroup generators to make the paper self-contained. We start with the notion of an *observable*. Observables are mappings that take a time-domain signal as input and produce a scalar number as output. The mean $\mu(x)$, energy $E(x)$ and value $V_0(x)$ at zero of a signal $x = x(\tau)$ are classic examples for observables:

$$\mu(x) = \int_{-\infty}^{\infty} x(\tau)d\tau,\ E(x) = \int_{-\infty}^{\infty} |x(\tau)|^2 dt,\ V_0(x) = x(0).$$

Koopman operators describe how observables change when the signal evolves under a given PDE of the form

$$u_z = W(u), \quad u = u(\tau, z), \quad \tau \in \mathbb{R},\ z \geq 0, \tag{3}$$

where the variables τ and z indicates time and space, respectively, and W is a nonlinear operator. For example, the NLSE (1) is obtained using $W(u) = -\frac{\alpha}{2}u - i\frac{\beta_2}{2T_0^2}u_{\tau\tau} + i\gamma|u|^2\ u$. Technically, the Koopman operator maps observables to observables. The new observable first uses the PDE to evolve the given signal from the location zero to the location z and then evaluates the old observable at the evolved signal (Fig. 1). For example, if $E(x)$ is again the energy of the signal $x(\tau)$, then $K^zE(x)$ is the energy of the signal $u(z, \tau)$ that we obtain by solving the PDE with the initial condition $u(\tau, 0) = x(\tau)$. Although the observables themselves can be nonlinear, the Koopman operator, as a mapping of observables to observables turns out to be linear. The linear nature of the Koopman operator enables us to

investigate the underlying *nonlinear* PDE through the analysis of *linear* operators if we can handle the infinite-dimensional problem in some reasonable way.

The action of the Koopman operator obviously depends on the chosen propagation distance z. In fact, we obtain a different Koopman operator K^z for each $z \geq 0$. This family of Koopman operators has a specific structure, known as *semigroup* [11]. That is,

$$K^{z_2}K^{z_1} = K^{z_1+z_2}, \quad K^0 = I,$$

where I is the identity operator. Note that these equations simply reflect that the PDE is space-invariant. It does not matter if we first evolve $u(\tau,0) = x(\tau)$ to $y(\tau) = u(\tau, z_1)$ and then $u(\tau,0) = y(\tau)$ to $u(\tau, z_2)$, or if we directly evolve $u(\tau,0) = x(\tau)$ to $u(\tau, z_1 + z_2)$. In both cases, we get the same result. Many semigroups, including the one here, can be described through a single operator known as *generator*. The generator L again maps observables to observables, but does not depend on the propagation distance z. It is sufficient to describe the whole semigroup, which is recovered from the generator using the exponential function for operators:

$$K^z = \exp(Lz) = \sum_{n=0}^{\infty} \frac{z^n}{n!} L^n, \quad L^n\xi = \underbrace{L(L(\dots L(\xi)))}_{n \text{ applications}}. \tag{4}$$

With this formula, one finds that the generator is given by

$$\begin{aligned} L &= \lim_{z\to 0} \frac{(I + \frac{z^1}{1}L^1 + \frac{z^2}{2}L^2 + \dots) - I}{z} \\ &= \lim_{z\to 0} \frac{\exp(Lz) - I}{z} = \lim_{z\to 0} \frac{K^z - I}{z}. \end{aligned} \tag{5}$$

For details on the theory presented here, we refer to [15], [18].

The spaces of observables are normally infinite-dimensional, which makes their numerical treatment difficult. In practice, one typically works with a finite-dimensional subspace. We can then define a projection operator P_n that leaves observables in the subspace unchanged but maps observables outside the subspace to approximations inside it. With this projection, finite-dimensional approximations

$$K_n^z = P_n K^z P_n, \quad L_n^z = P_n L P_n \tag{6}$$

of the Koopman operators and their generator, respectively, are introduced. Let now $\xi_1, \dots, \xi_n$ be a basis for the finite-dimensional subspace. When we apply the approximated Koopman operators or the approximated generator to the individual basis functions, the resulting outputs are again in the subspace by construction. We expand them in the basis:

$$K_n^z\xi_j = \sum_{k=1}^{n} \mathbf{K}_{kj}\xi_k, \quad L_n\xi_j = \sum_{k=1}^{n} \mathbf{L}_{kj}\xi_k, \quad j = 1, \dots, n. \tag{7}$$

The coefficient matrices $\mathbf{K} = [\mathbf{K}_{kj}]$ and $\mathbf{L} = [\mathbf{L}_{kj}]$ specify the approximated Koopman operators and generator completely. We illustrate this for the approximated Koopman operators. Let $\xi = \sum_{k=1}^{n} a_k\xi_k$ be any input in the subspace. Then,

$$K_n^z\left(\sum_{k=1}^{n} a_k\xi_n\right) = \sum_{k=1}^{n} a_k K_n^z\xi_n = \sum_{k=1}^{n} a_k \sum_{m=1}^{n} \mathbf{K}_{mj}\xi_m.$$

We again refer to [11] and there references therein for further details. Finding the finite-dimensional coefficient matrices describing the approximated Koopman operators from data is one of the main goals in the recent literature. See e.g. the extended dynamic mode decomposition algorithm [19].

B. Koopman-Based Identification Method

We now explain the KIM method tailored to the NLSE. We recall that the NLSE (1) can be written in the form (3):

$$u_z = \sum_{k=1}^{3} c_k W_k(u) = c_1 u + c_2 u_{\tau\tau} + c_3|u|^2 u. \tag{8}$$

The coefficients c_k can be complex and related to the usual loss, dispersion and Kerr parameters by

$$c_1 = -\frac{\alpha}{2}, \quad c_2 = -i\frac{\beta_2}{2T_0^2}, \quad c_3 = i\gamma. \tag{9}$$

Since we know the form of the NLSE, we can consider this problem as a parameter estimation problem where the KIM estimates the coefficients c_k from m data-pairs $\{u^j(\tau, z=0), u^j(\tau, z = Z)\}_{j=1}^m$ of fiber inputs and corresponding outputs. The fiber span length is denoted by Z.

The theoretical insight behind the KIM is that the first column of the coefficient matrix $\mathbf{L}$ for the approximated generator approximates the coefficients c_k of the PDE [11, Prop. 1]. (We will motivate this result below, after all necessary notions have been introduced.) The main task is thus to estimate the matrix $\mathbf{L}$ from the data. The KIM, whose steps are illustrated in Fig. 2, first estimates the coeffient matrix of the approximated Koopman operator, $\mathbf{K}$. Following [11], we choose observables of the form $\xi_k(u) = \langle W_k(u), w\rangle$, where $w(\tau)$ is a Gaussian window function, the W_k are the library terms from the NLSE (8), given by $W_1(u) = u$, $W_2(u) = u_{\tau\tau}, W_3(u) = u|u|^2$, and $\langle f, g\rangle = \int f(\tau)\bar{g}(\tau)d\tau$ is the usual inner product. We then construct an input data matrix Θ_1 and an output data matrix Θ_2 from fiber inputs and outputs, respectively, using the basis of observables as shown in Fig. 2(b). Once we have input and output data matrices, we approximate the projected Koopman operator in (7) by solving the minimization problem

$$\min_{\mathbf{K}\in\mathbb{C}^{3\times 3}} \|\Theta_2 - \Theta_1\mathbf{K}\|_F^2, \tag{10}$$

where $||\cdot||_F$ is the Frobenius norm. The matrix approximation of the Koopman operator (7) is then given by the least squares solution $\mathbf{K} = \Theta_1^\dagger\Theta_2$, where $\Theta_1^\dagger$ is the Moore-Penrose pseudoinverse. Following the connection in (4), the projection of the generator can be approximated as $\mathbf{L} = \frac{1}{Z}\operatorname{Log}(\mathbf{K})$, where Log is the matrix logarithm.

Proposition 1 in [11] now states that the first column of $\mathbf{L}$ approximates the desired coefficients c_k for the PDE. This can be seen as follows. Using that $K_z\xi_1(u(\tau,0)) = \xi_1(u(\tau,z))$ by definition of the Koopman operator, the generator (5) applied to

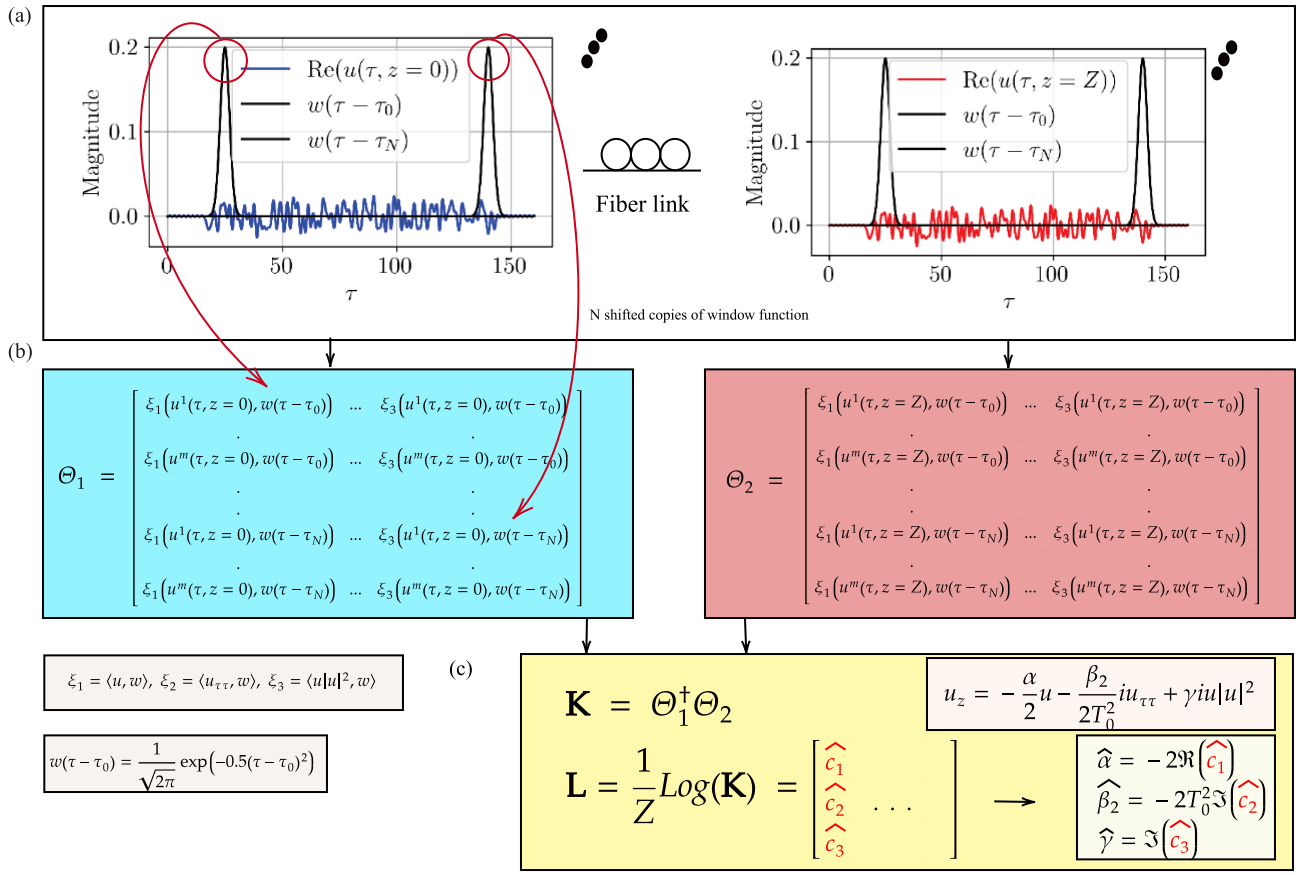

Fig. 2. Illustration of the Koopman-based Fiber Parameter Identification Method. The hats (ˆ) indicate estimates.

the observable $\xi_1(u) = \langle u, w\rangle$ is found to satisfy

$$\begin{aligned} L\xi_1(u) &= \lim_{z\to 0} \frac{\langle u(\tau,z), w\rangle - \langle u(\tau,0), w\rangle}{z} \\ &= \langle u_z(\tau,0), w\rangle \\ &\overset{(8)}{=} c_1\langle W_1(u), w\rangle + c_2\langle W_2(u), w\rangle + c_3\langle W_3(u), w\rangle. \end{aligned}$$

On the other hand, we also have

$$\begin{aligned} L\xi_1(u) &\approx L_n\xi_1(u) \\ &= \boldsymbol{L}_{11}\xi_1(u) + \boldsymbol{L}_{21}\xi_2(u) + \boldsymbol{L}_{31}\xi_3(u) \\ &= \boldsymbol{L}_{11}\langle W_1(u), w\rangle + \boldsymbol{L}_{21}\langle W_2(u), w\rangle \\ &\quad + \boldsymbol{L}_{31}\langle W_3(u), w\rangle. \end{aligned}$$

Comparing these two expressions for the generator applied to the observable ξ_1 implies that indeed $c_k \approx \boldsymbol{L}_{k1}$. Proposition 1 in [11] also shows that the KIM recovers the true coefficients in the limit $Z \to 0$ in the noise-free case, given a sufficiently rich data set. It is pointed out in [11] that accurate estimates can also be obtained if Z is not small. However, the method will eventually break down when Z is too large. We are therefore interested in if it is suitable for fiber identification.

We can summarize the steps in the KIM as follows:

1) Collect m input-output data pairs $\{u^j(\tau, z=0), u^j(\tau, z=Z)\}_{j=1}^m$ as shown in Fig. 2(a)
2) Build data matrices Θ_1 and Θ_2 as shown in Fig. 2(b)
3) Construct the matrix $\mathbf{K} = \Theta_1^\dagger\Theta_2$ (Fig. 2(c))
4) Compute the matrix $\mathbf{L} = \frac{1}{Z}\mathrm{Log}(\mathbf{K})$. The first column of $\mathbf{L}$ approximates the c_k (Fig. 2(c)).

Note that the KIM does not require the computation of spatial derivatives. Furthermore, there are fast and numerically reliable methods to update the Koopman matrix $\mathbf{K}$ when new data becomes available or old data should be removed [20].

TABLE I
GROUND TRUTH PARAMETERS OF THE DIFFERENT FIBER TYPES

Fiber Type	α, (db/km)	β_2, (ps^2/km)	γ, (1/Wm)
SRS	0.215	3.95	$2.18\cdot10^{-3}$
TrueWave RS	0.230	−5.10	$1.99\cdot10^{-3}$
Metrocore	0.250	9.69	$2.12\cdot10^{-3}$
SSMF	0.200	−21.7	$1.37\cdot10^{-3}$

IV. Simulation Setups

We identify the parameters α, β_2 and γ for the NLSE (1) and the Manakov equations (2) for a fiber-optic link with one span followed by an (EDFA) with a 6 dB noise figure. We vary the span length and transmit powers. For each length, we estimate the fiber parameters of four different fiber types shown in Table I [21].

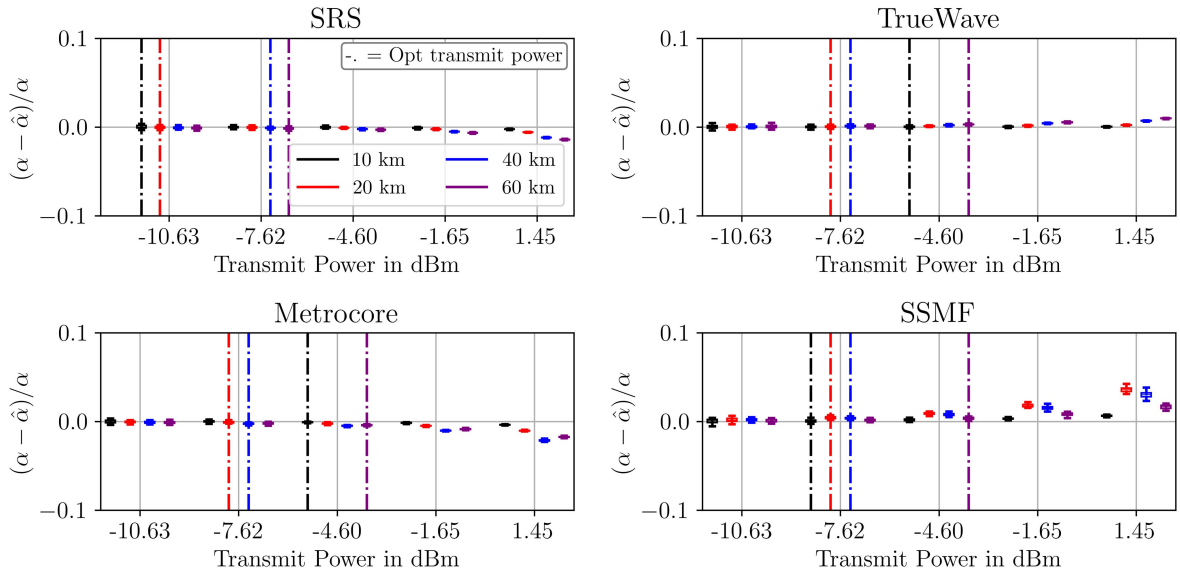

Fig. 3. Relative errors in attenuation parameter, α, of transmit power for different span lengths and different fibers with 6 dB EDFA noise.

A. Simulation Setup for the Nonlinear Schrödinger Equation

The normalization constant is $T_0 = 25$ ps, which ensures that c_2 has a magnitude of the same order as c_1 and c_3. The input-output data was obtained using the current development version of NFDMLab [22] (commit 361e23c). The step sizes dz and $d\tau$ for the underlying Fourier split step method are chosen to be 0.5 km and 0.065, respectively. The fiber inputs were generated using Nyquist pulse-shaping with raised cosine pulses (roll-off 0.1) and a symbol spacing, T_s, of 25 ps. Fiber inputs consisted of 128 16-QAM and 32 guard symbols and were ideally low-pass filtered at 40 GHz bandwidth before transmission. The same filter was applied at the receiver. One input-output pair is shown in Fig. 2(a). We remove the amplifier gain from the fiber output before the identification. The candidate term $W_2 = u_{\tau\tau}$ is approximated by the 4th order accurate central finite difference approximation with uniform grid spacing. The boundary points are treated by the 4th order accurate forward finite difference. We choose a Gaussian weighting function, $w(\tau - \tau_n) = 1/\sqrt{2\pi}\exp(-0.5(\tau - \tau_n)^2)$, when computing the inner products in Fig. 2(b). Note that the window function used for the construction of data matrices is narrow, so that it is somewhat close to a delta pulse. With an actual delta pulse, the data matrix would simply contain samples of the signals. We additionally applied shifted versions of the window function to extract more data from each pulse, as shown in Fig. 2(a). We mention that the τ_n are on an equidistant grid with $\tau_0 = 25$, $\tau_N = 140$, and $N = 115$. We made the selection such that it covers the entire signal except the guard band. We note that Θ_1 and $\Theta_2 \in \mathbb{C}^{mN\times 3}$, where N is the number of shifted window functions. We used $m = 90$ input-output data pairs per identification.

B. Simulation Setup for Manakov Equations

We keep the same simulation setup for both equations except for the identification of the Manakov equations, we adapted the KIM by incorporating the additional library terms from the Manakov equations, explicitly stating $W_1 = u$, $W_2 = u_{\tau\tau}$, $W_3 = u(|u|^2 + |v|^2)$, $W_4 = v$, $W_5 = v_{\tau\tau}$, and $W_6 = v(|u|^2 + |v|^2)$, to construct our data matrices. Therefore, now the data matrices Θ_1 and $\Theta_2 \in \mathbb{C}^{mN\times 6}$. The respective columns of the matrix approximation $\mathbf{L}$ (the first column corresponding to the first polarization $W_1 = u$ and the fourth column corresponding to the second polarization $W_4 = v$) contain the approximate coefficients.

V. Results and Discussion

A. Parameter Identification for the Nonlinear Schrödinger Equation

The results of the simulations are shown in the Figs. 3–5, where the dependence of the signed relative errors in the parameter estimates (e.g., $(\alpha - \hat{\alpha})/\alpha$ for α in Fig. 3) are shown as a function of the transmit power for the link lengths of 10, 20, 40 and 60 km for each of the considered fiber types. The boxplots in each figure show errors in 50 estimates of $\hat{\alpha}$, $\hat{\beta}_2$, and $\hat{\gamma}$. In order to read the boxplots, we note that they show the mean and the variance of signed relative error at each transmit power. The lower end of the box represents 1st quartile of the data, the upper end represents 3rd quartile, whereas ends of the whiskers represent the maximum and minimum of the data. In some cases (e.g. Fig. 3), the boxplots seem to be collapsed to a single line because of low variance. The optimal transmit powers, at which the error vector magnitude (EVM) at the receiver (with an additional dispersion compensation block) are minimal, are marked with dashed vertical lines in Fig. 3 for each fiber type. We note that the optimal transmit powers for different lengths and fiber types may differ slightly in some cases. However, the performance of the fiber link remains very close to the optimum transmit power up to transmit power of ≈ -4.5 dBm. Only after that the EVM starts to increase. Therefore, we can consider the differences as outliers.

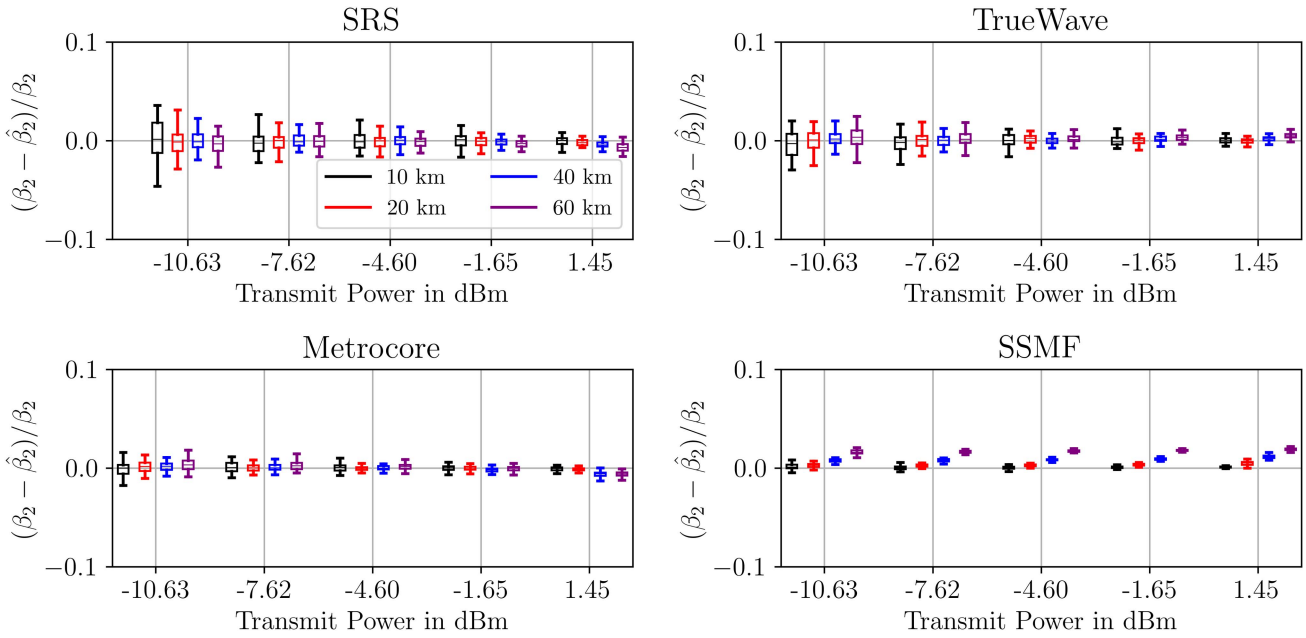

Fig. 4. Relative errors in dispersion parameter, β_2, of transmit power for different span lengths and different fibers with 6 dB EDFA noise.

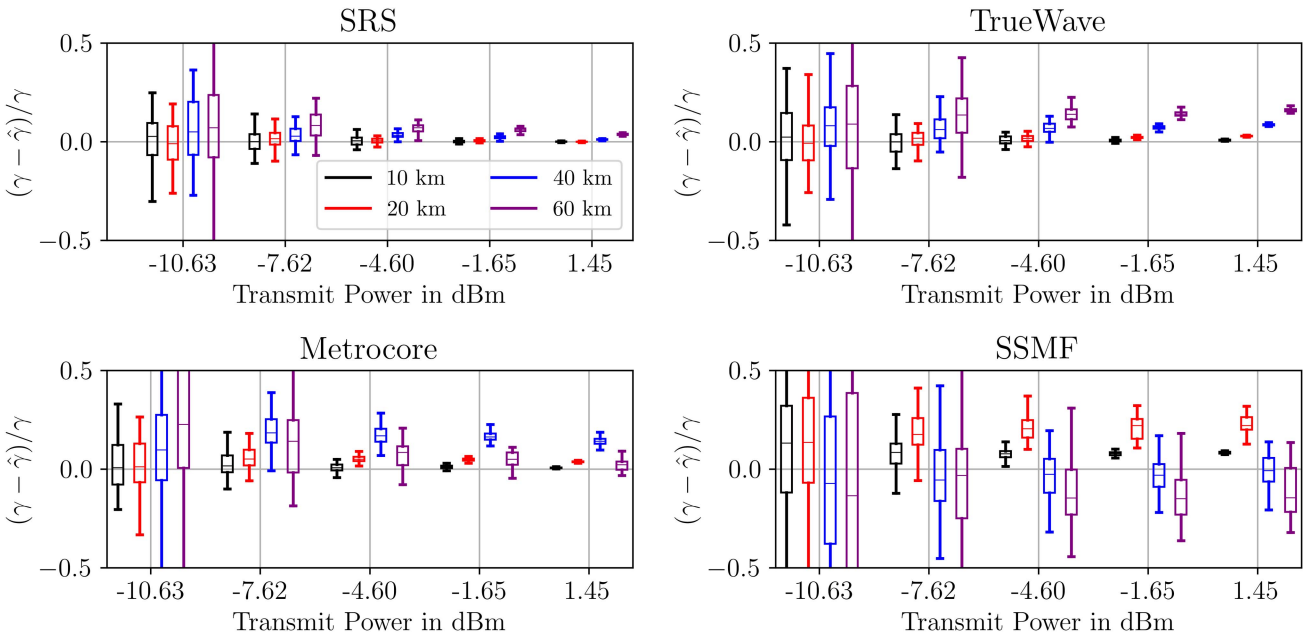

Fig. 5. Relative errors in the Kerr nonlinearity parameter, γ, of transmit power for different span lengths and different fibers with 6 dB EDFA noise.

We observe that the identification of the loss parameter α and dispersion parameter β_2 succeeded for all considered span lengths and transmit powers, with relative errors very close to zero. The maximum relative error for both α and β_2 stays below 5.0%. We also see that the variance stays the same, and the error comes in the form of bias. The identification of the Kerr parameter γ is more difficult. Therefore, we have selected a plot range of $(-0.5, 0.5)$ for this case. For all span lengths, we observe that the transmit power reduces the variance of the estimates. Increasing the transmit power makes the identification of γ better as the nonlinear term in the NLSE becomes more dominant. This is in contrast to α and β_2, which are linear terms that become more difficult to identify at high powers for the same reason. (For the SRS, TrueWave and Metrocore fibers in Fig. 4 this effect is less obvious because there is a second effect at play. At low powers, increasing power will improve results also for α and β_2 up to a certain point because the signal-to-noise ratio increases while the impact of γ is not yet dominant.) Moreover, we observe

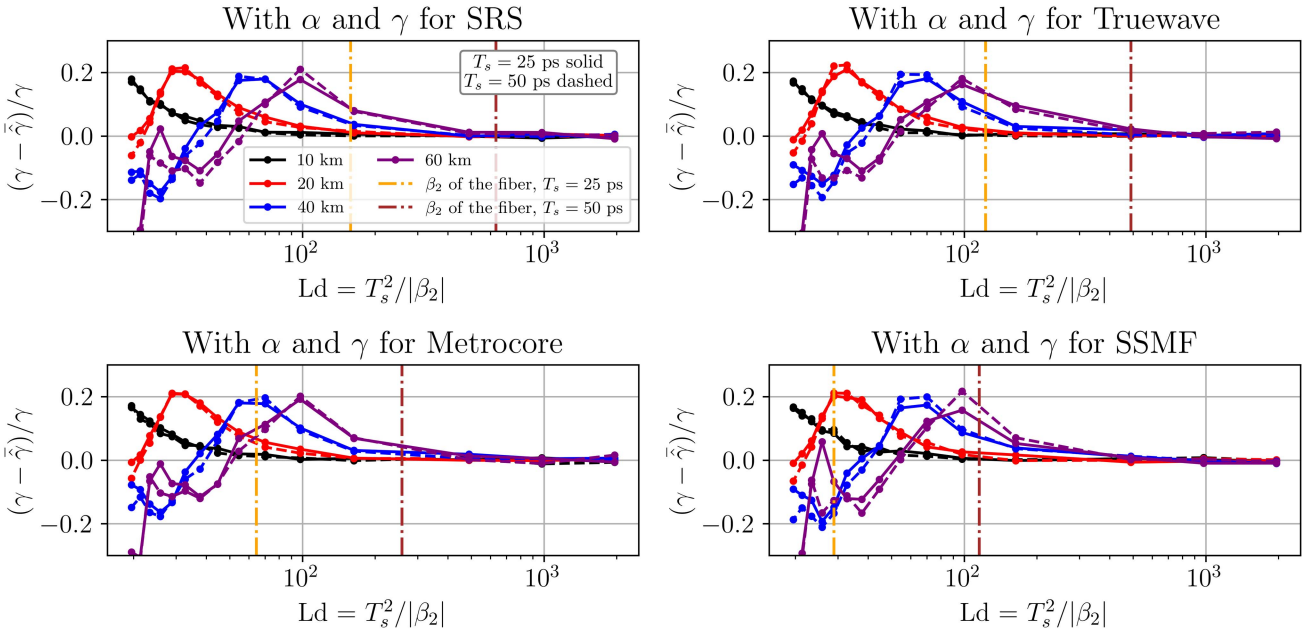

Fig. 6. Mean relative error in the Kerr nonlinearity parameter, γ, of dispersion lengths, $L_d = T_s^2/|\beta_2|$. Transmit power ≈ -4.5 dBm. Two symbol spacing considered $T_s = 25$ ps (solid lines) and $T_s = 50$ ps (dashed lines).

that the identification of γ is quite different for different fiber types. The identification of γ for SSMF and metro-core fiber (see bottom two figures in Fig. 5), which have larger dispersion coefficients, has more bias and variance at comparable transmit powers than the SRS and Truewave fiber (see top two figures in Fig. 5), which have lower dispersion coefficients. It indicates that γ is identified better when the effect of dispersion is weak as compared to the effect induced by the nonlinearity. Fig. 6 shows the dependence of the mean relative error (mean taken from 50 estimates) in γ against the dispersion length, $T_s/|\beta_2|$, where T_s is the symbol spacing, which also controls the bandwidth of the signal. To change the dispersion length, we selected $T_s = 25$ ps and $T_s = 50$ ps, and swept for different $|\beta_2|$ values. For the first case, the range of $|\beta_2|$ chosen is from 0.319 to 31.9 ps^2/km. For the second case, the range is from 1.28 to 128 ps^2/km. We used these different ranges to keep the range of dispersion lengths the same in both cases. Dispersion length corresponding to each of the $|\beta_2|$ value of the four fibers is shown by orange ($T_s = 25$ ps) and brown ($T_s = 50$ ps) dash-dot lines in the respective sub-figures of Fig. 6. As we see from Fig. 6, the relative errors for all the four γ values considered approach zero when the dispersion length is quite large (see, for example, $L_d = 10^3$ km) as compared to the link length. As the dispersion length and the link length become closer, the identification of γ becomes more difficult. The different identification result of γ parameter in Fig. 5, that the identification in SRS and Truewave fiber is much better than identification in SSMF and Metrocore fiber, can be explained by this. Finally, note that the corresponding curves in the four panels of Fig. 6 are very similar for the all fiber types, which suggests that the dispersion length is the main parameter influencing the performance of the KIM.

By comparison with the noise-free case shown in Fig. 7, we see that noise is the limiting factor for the identification of γ in the low-power regime. Moreover, the noise introduces a lot of variance in the identification of γ. Interestingly, the identification of α and β_2 is affected much less by the noise (as the errors for the noisy case are already close to zero). We see the effect of dispersion length on the identification of γ in the noiseless case as well. The performance of the KIM for γ estimates for SSMF and Metrocore fiber is poor, even in the noiseless case. At transmit powers ≈ -4.5 dBm (which is near optimal for all cases), the KIM is always able to identify γ with relative errors not exceeding 20%. However, if we increase the symbol spacing, T_s, which will reduce the signal bandwidth, we can identify γ with much better accuracy for all the fibers. We can thus conclude that the KIM is suited to identify the fiber parameters jointly for the considered span lengths.

B. Comparison of KIM Against Other Parameter Estimation Techniques for the γ Parameter

We also compared the KIM against two other methods for the identification of γ: matching of conserved quantities (see the appendix of [6]), and a direct identification method similar to SINDy [4], [23] (except for the sparsity promotion, which is not necessary in our case, because we exactly know which coefficients we want to identify), where we approximated the spatial derivatives only from the input and output signals in Fig. 8. Note that in contrast to the KIM, these benchmarks require the values of α and β_2 in order to estimate γ. With the direct method, the coefficients are approximated as

$$\hat{C} = \Theta_1^{\dagger}[\langle \dot{u}^1, w\rangle, \langle \dot{u}^2, w\rangle, \ldots, \langle \dot{u}^m, w\rangle]^T,$$

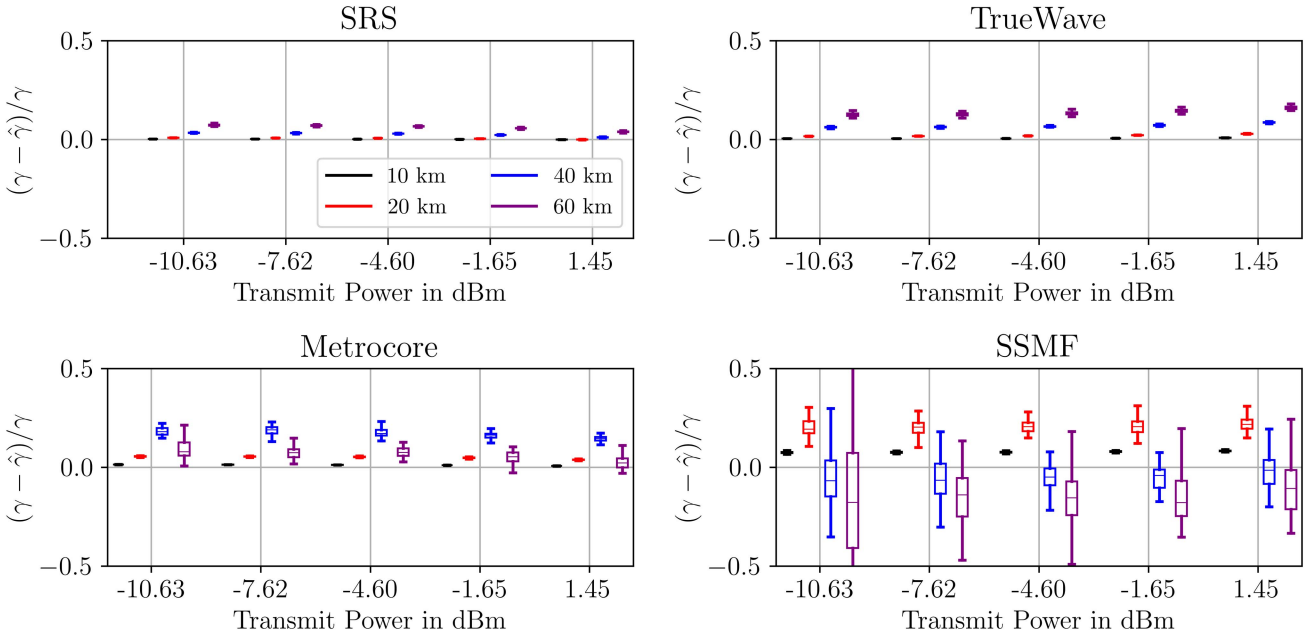

Fig. 7. Relative errors in the Kerr nonlinearity parameter, γ, of transmit power for different span lengths and different fibers with no EDFA noise.

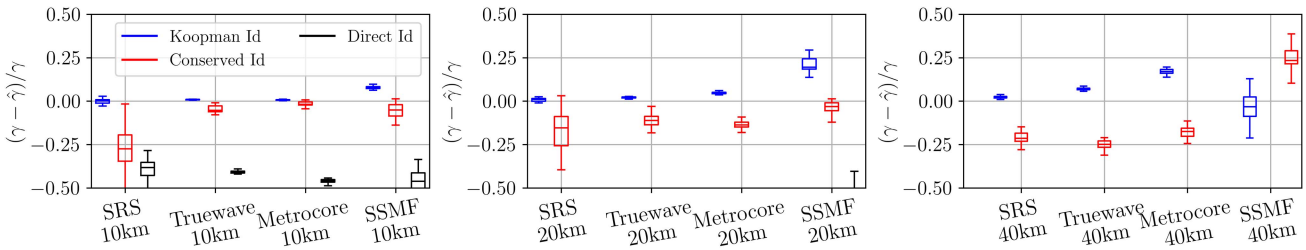

Fig. 8. Comparison between KIM, conserved quantities identification, and SINDy for Kerr nonlinearity at high transmit power for 10 km, 20 km, and 40 km link length.

where $\dot{u}^m = \frac{u^m(\tau, z=Z) - u^m(\tau, z=0)}{Z}$ is a finite difference approximation of the spatial derivative of u. For the comparison, we kept the transmit power relatively quite high at ≈ 1.45 dBm. We observe that SINDy type identification fails even for 10 km. However, the results from the KIM and conserved quantities are relatively comparable. For 10 and 20 km, Koopman outperforms conserved quantities identification. At 40 km, KIM starts to introduce bias in the identification, but the performance still remains comparable. We again note that the conserved quantities identification method relies on the prior knowledge of β_2 to estimate γ, but the KIM jointly identifies all the parameters involved.

C. Dependency of the Performance of the KIM on the Number of Input-Output Data Pairs

We now investigate the dependency identification error of the Kerr parameter, γ, on of the number of input-output data pairs. We increase the number of input-output pairs m in the data set $\{u^j(\tau, z=0), u^j(\tau, z=Z)\}_{j=1}^m$ from $m = 30$ to $m = 270$ in steps of 30 and plot the signed relative error for $\hat{\gamma}$. We simulate the transmission in an SRS fiber at optimal transmit power. Fig. 10 shows the result of 100 estimates of $\hat{\gamma}$ for different link lengths. We can see that as the number of input-output data pairs increases, the variance in the error reduces. This is the expected result. We note that the variance of the error increases gracefully as m decreases. This suggests that m is not a sensitive parameter. Furthermore, we see that the bias introduced at larger link lengths does not change much with the number of data pairs. The results for the other fiber types show similar trends and can be found in the supplementary material.

D. Parameter Identification for the Manakov Equation

We also implemented the KIM method to estimate the parameters of Manakov equations (2). The results for α and β_2 are similar to the one for the nonlinear Schrödinger equation case, i.e the identification was successful (relative error stayed below 5%) for both α and β_2 for all the fibers considered and all the transmit powers. Due to space limitations, we omitted the figures. However, Fig. 9 shows the results for the identification of Kerr's nonlinearity parameter for the u polarization. We can

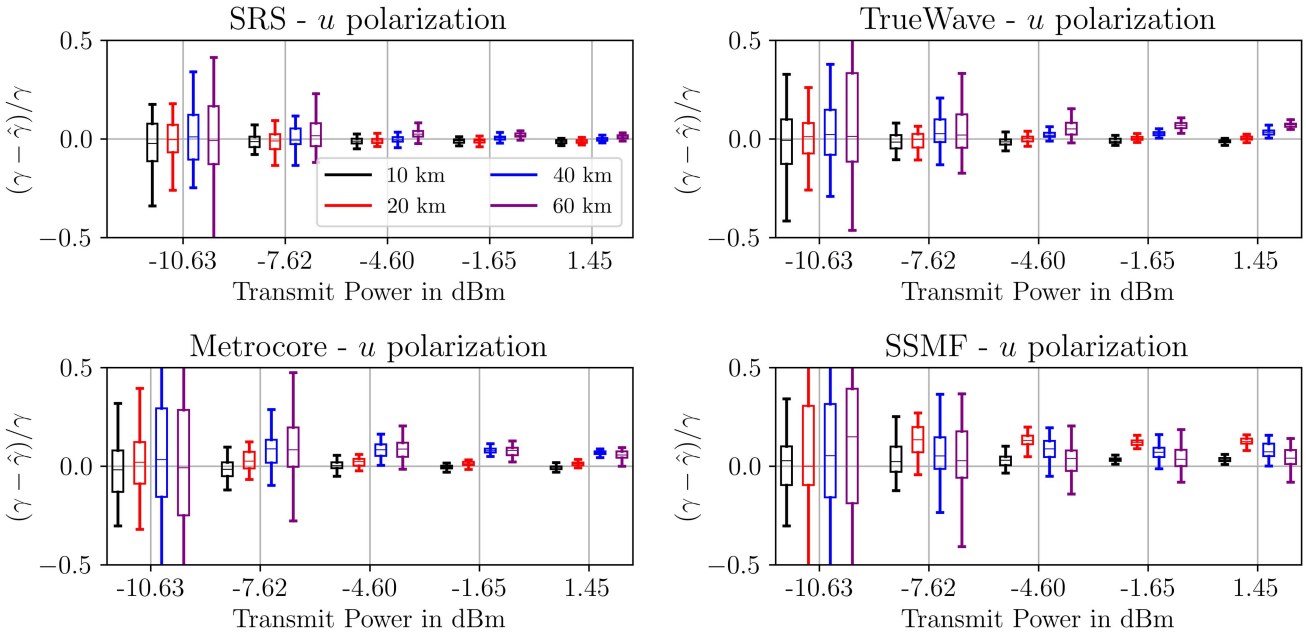

Fig. 9. Manakov equations (u polarization): Relative errors in the Kerr nonlinearity parameter, γ, of transmit power for different span lengths and different fibers with 6 dB EDFA noise.

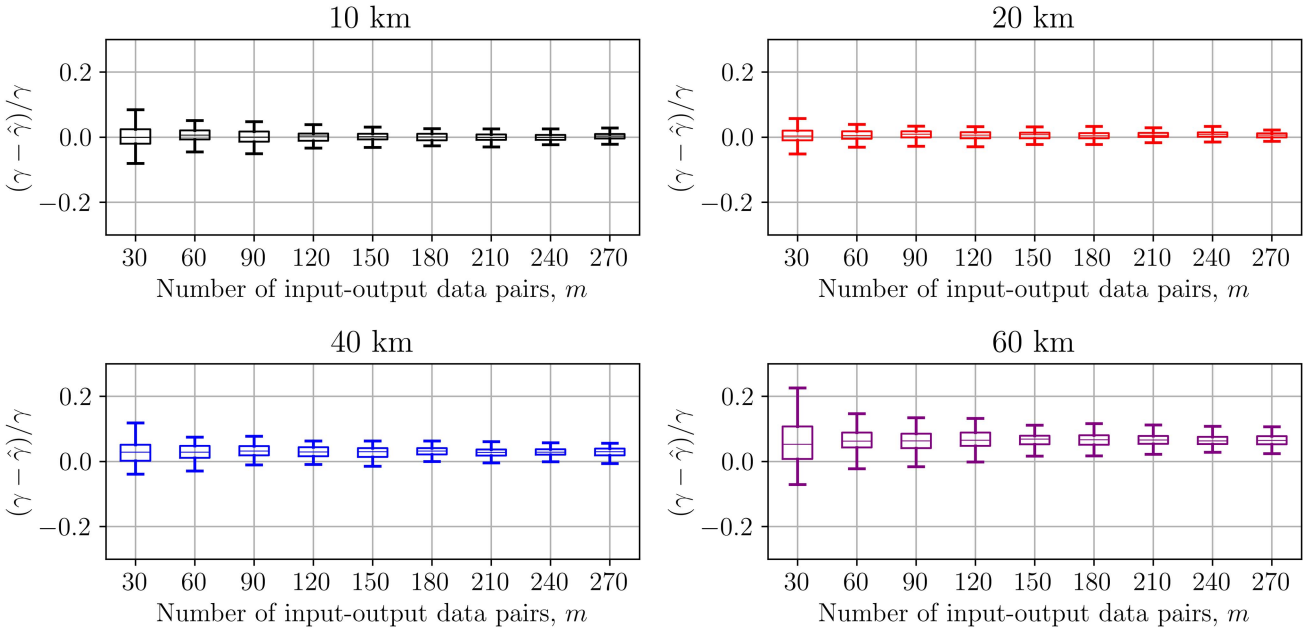

Fig. 10. Dependency of the relative error in the identified Kerr parameter, γ, on the number of input-output data pairs m for SRS fiber at optimal transmit power.

see that it follows similar trend as in the case of nonlinear Schrödinger equation. The results for the v polarization are similar and can be found in the supplementary material.

VI. Fiber Link Monitoring

In this section, we deal with the fiber parameter tracking problem. Our goal is to detect changes in the parameters of the nonlinear Schrödinger equation[1] (1). The motivation is that we hope that the changes in fiber parameters are less biased than the estimates of fiber parameters themselves. First, we determine initial estimates for α, β_2, and γ using the KIM as illustrated in Fig. 11(left). This would happen when the fiber link is deployed.

[1]The results for the Manakov equations are similar and can be found in the supplementary material. The supplementary material furthermore also contains results for the NLSE where the parameter changes have lower variances.

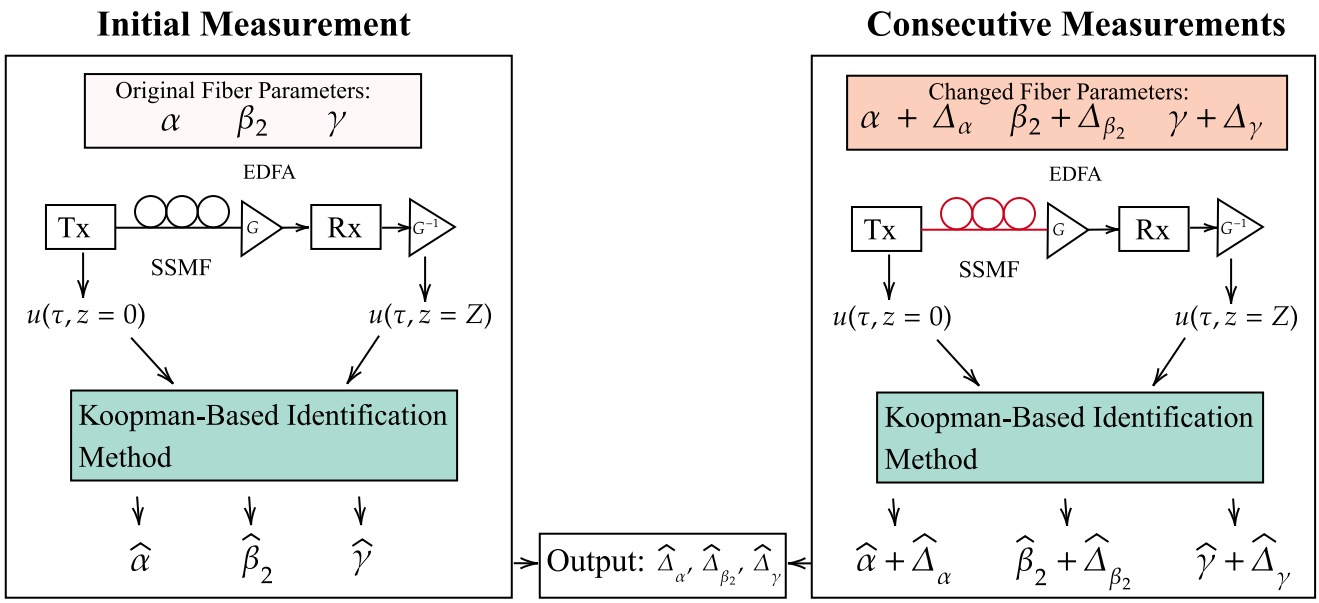

Fig. 11. Proposed method for tracking changes in an SSMF link. We estimate the changes Δ_α, Δ_{β_2}, and Δ_γ in the fiber parameters by applying the KIM twice. The hats ($\hat{}$) indicate estimates. The inverse gain G^{-1} is applied digitally.

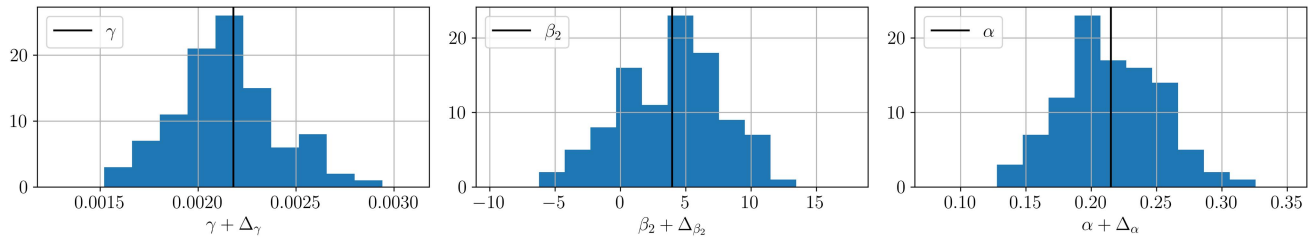

Fig. 12. Example of distribution of the changed fiber parameters in SRS fiber (same units as given in Table I).

The initial estimates are denoted $\hat{\alpha}$, $\hat{\beta}_2$, and $\hat{\gamma}$. Later, when the fiber is operational, we employ the KIM again to estimate the changed fiber parameters $\hat{\alpha} + \hat{\Delta}_\alpha$, $\hat{\beta}_2 + \hat{\Delta}_{\beta_2}$, and $\hat{\gamma} + \hat{\Delta}_\gamma$, as is illustrated in Fig. 11(right). By subtracting the initial from the current estimates for each parameter, we obtain estimates for the change in each fiber parameter, i.e., $\hat{\Delta}_\alpha$, $\hat{\Delta}_{\beta_2}$ and $\hat{\Delta}_\gamma$. If these differences become large, we can assume that the fiber parameters have changed.

A. Simulation Setup

We identify the changes Δ_α, Δ_{β_2} and Δ_γ in the parameters for 60 and 80 km fiber-optic links with one span followed by an EDFA with a 6 dB noise figure. We consider two transmit powers: optimal transmit power for a receiver with chromatic dispersion compensation (≈ -5 dBm) and a high transmit power (≈ -2.5 dBm). The initial ground truth parameters are given in Table I. The data generation process is the same as described in the Section IV.

We estimate changes in the fiber parameters for 100 different random updates. Each time, the ground truth parameters given before underwent a different random change in the parameter values. That is, the initial parameters α, β_2, and γ are changed by some random Δ_α, Δ_{β_2}, and Δ_γ, respectively. The random changes are drawn from zero-mean normal distributions. The standard deviations σ for these changes are chosen to be $1/5^{th}$ of the actual parameter values. The distributions of the resulting fiber parameters are shown in Fig. 12. For each of the 100 parameter updates, 50 estimates of $\hat{\alpha}$, $\hat{\beta}_2$ and $\hat{\gamma}$, as well as $\hat{\Delta}_\alpha$, $\hat{\Delta}_{\beta_2}$ and $\hat{\Delta}_\gamma$ were averaged. These averages are indicated with a bar, e.g. $\bar{\hat{\alpha}}$ or $\bar{\hat{\Delta}}_\alpha$. For each run of the KIM, 90 input-output data pairs were used.

B. Results

The results of the simulations are presented in the Figs. 13 and 14, where the relative errors in the average parameter estimates (e.g., $\frac{\alpha - \bar{\hat{\alpha}}}{\alpha}$ for α) and, respectively, in the average parameter changes (e.g., $\frac{\Delta_\alpha - \bar{\hat{\Delta}}_\alpha}{\alpha}$ for Δ_α) are summarized for the 100 different parameter changes, for 60 and 80 km links, at optimal (≈ -4.60 dBm) and high transmit power (≈ -1.65 dBm). The y-axes in the plots range from -20% to 20%.

Fig. 13 demonstrates the aforementioned bias in the plain KIM. We observe that the estimated value of the Kerr parameter γ is biased in all the scenarios. The biases range from 3.83% (80 km at high power for Metrocore) to 19.2% (80 km at high power

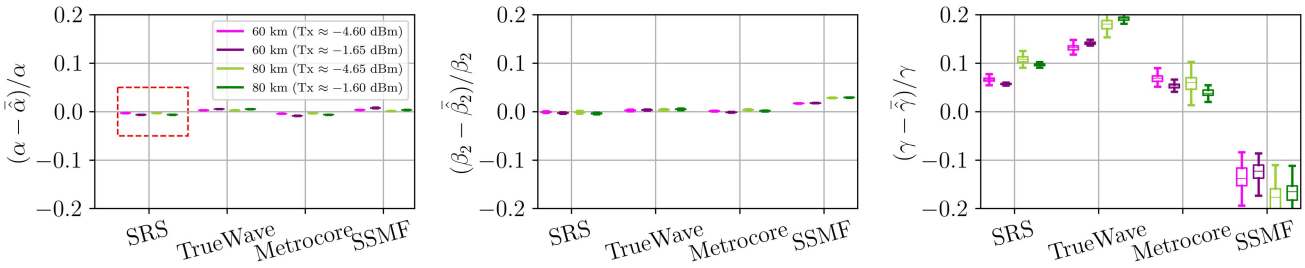

Fig. 13. Results for the plain KIM method (direct estimation of fiber parameters).

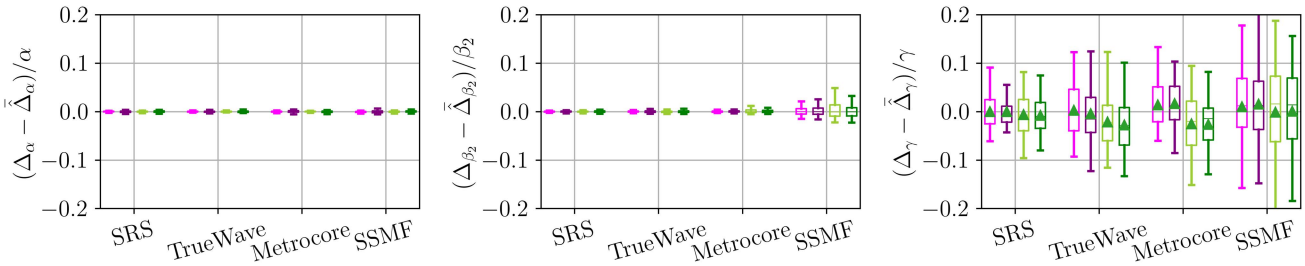

Fig. 14. Results for the proposed method (estimation of changes in the fiber parameters).

for Truewave) of the true value. Higher transmit power reduces the variance, which can be explained by the fact that the effect of the Kerr nonlinearity grows with the transmit power. We also observe that the dispersion parameter β_2 and the loss coefficient α are identified accurately at optimal and high transmit power with biases below 3%.

Fig. 14 shows the results for the proposed parameter change estimation method. We observe that changes in the Kerr parameter Δ_γ are estimated much better and that the bias is significantly reduced in the estimated values of Δ_γ for all scenarios. All biases are now below 3% of the true value (shown by the triangle in Fig. 14). The smallest improvement is seen in the case of Metrocore fiber, and the bias is improved by a factor of 1.5. Whereas the most improvement is seen in the case of SRS fiber, where the bias is improved by a factor of 12.3. Higher transmit power improves the estimation of changes in the Kerr parameter as well. Similarly, we see that changes in the dispersion parameter Δ_{β_2} and loss coefficient Δ_α are estimated accurately in all scenarios, with biases below 0.15%.

We can thus conclude that changes in *all* of the parameter were estimated accurately for link lengths up to 80 km, even though the identified Kerr parameters themselves were biased and not accurate at these distances.

VII. Conclusion

We investigated the suitability of a Koopman-based parameter identification method for optical fiber spans. The method uses only input-output data from an operational link (and thus, no special probing signals or hardware). Moreover, the method does not require spatial derivatives but nevertheless deteriorates as the span length increases. We investigated the span lengths 10, 20, 40, and 60 km of four different fiber types. For the considered transceiver, the method was always able to identify α and β_2 with negligible error. It was also able to identify γ for all link lengths, with low relative errors, at optimal transmit power. We noticed that the identification of γ performs differently for different fiber types. The dispersion length was identified as the critical factor contributing to the accuracy. We also compared the Koopman-based identification method with other fiber parameter estimation techniques and showed that the proposed method performs better than other methods at considered span lengths. We also proposed to monitor *changes* in the fiber parameters of single-span links using the Koopman-based identification method instead of the parameters themselves. Such changes indicate a need for re-calibration or even maintenance. Although the estimated Kerr nonlinearity parameter provided by the KIM exhibited a bias already for links of 40 km, we surprisingly observed that changes in the Kerr parameter nevertheless were estimated accurately for links of 60 and 80 km. Our approach thus extends the applicability of the KIM for monitoring purposes considerably. Future research should investigate if the reach of the method can be improved and if it can be extended to links with multiple spans. Experimental verification of the method should also be considered as a topic for future study.

References

[1] S. Aamir and S. Wahls, "Evaluation of Koopman-based fiber parameter estimation," in *Proc. 49th Eur. Conf. Opt. Commun.*, 2023, pp. 1370–1373.

[2] S. Aamir and S. Wahls, "Fiber parameter change monitoring in single span SSMF links using Koopman operators," in *Proc. 50th Eur. Conf. Opt. Commun.*, 2024, pp. 1370–1373.

[3] B. Batagelj, "Review of so far proposed fiber n/sub 2/measurement schemes," in *Proc. 4th Int. Conf. Transparent Opt. Netw.*, 2002, pp. 103–106.

[4] S. L. Brunton, J. L. Proctor, and J. N. Kutz, "Discovering governing equations from data by sparse identification of nonlinear dynamical systems," *Proc. Nat. Acad. Sci. USA*, vol. 113, no. 15, pp. 3932–3937, 2016.

[5] S. H. Rudy, S. L. Brunton, J. L. Proctor, and J. N. Kutz, "Data-driven discovery of partial differential equations," *Sci. Adv.*, vol. 3, no. 4, 2017, Art. no. e1602614.
[6] P. De Koster and S. Wahls, "Dispersion and nonlinearity identification for single-mode fibers using the nonlinear Fourier transform," *J. Lightw. Technol.*, vol. 38, no. 12, pp. 3252–3260, Jun. 2020.
[7] P. De Koster, J. Koch, O. Schulz, S. Pachnicke, and S. Wahls, "Experimental validation of nonlinear Fourier transform-based Kerr-nonlinearity identification over a 1600 km SSMF link," in *Proc. Opt. Fiber Commun. Conf.*, 2022, pp. W2A–39.
[8] C.-Y. Lin et al., "Adaptive digital back-propagation for optical communication systems," in *Proc. Opt. Fiber Commun. Conf.*, 2014, pp. M3C–4.
[9] M. Piels, E. P. da Silva, D. Zibar, and R. Borkowski, "Performance emulation and parameter estimation for nonlinear fibre-optic links," in *Proc. 21st Eur. Conf. Netw. Opt. Commun.*, 2016, pp. 1–5.
[10] X. Jiang, D. Wang, X. Chen, and M. Zhang, "Physics-informed neural network for optical fiber parameter estimation from the nonlinear Schrödinger equation," *J. Lightw. Technol.*, vol. 40, no. 21, pp. 7095–7105, Nov. 2022.
[11] A. Mauroy, "Koopman operator framework for spectral analysis and identification of infinite-dimensional systems," *Mathematics*, vol. 9, no. 19, 2021, Art. no. 2495.
[12] A. Mauroy and J. Goncalves, "Koopman-based lifting techniques for nonlinear systems identification," *IEEE Trans. Autom. Control*, vol. 65, no. 6, pp. 2550–2565, Jun. 2020.
[13] B. O. Koopman, "Hamiltonian systems and transformation in Hilbert space," *Proc. Nat. Acad. Sci. USA*, vol. 17, no. 5, pp. 315–318, 1931.
[14] A. Mauroy, Y. Susuki, and I. Mezić, *Koopman Operator in Systems and Control*. Berlin, Germany: Springer, 2020.
[15] S. L. Brunton, M. Budišić, E. Kaiser, and J. N. Kutz, "Modern Koopman theory for dynamical systems," *SIAM Rev.*, vol. 64, no. 2, pp. 229–340, 2022.
[16] G. P. Agrawal, *Fiber-Optic Communication Systems*. Hoboken, NJ, USA: Wiley, 2012.
[17] S. V. Manakov, "On the theory of two-dimensional stationary self-focusing of electromagnetic waves," *Zhurnal Eksperimentalnoi i Teoreticheskoi Fiziki*, vol. 65, pp. 505–516, Aug. 1973.
[18] H. Nakao and I. Mezić, "Spectral analysis of the Koopman operator for partial differential equations," *Chaos Interdiscipl. J. Nonlinear Sci.*, vol. 30, no. 11, 2020, Art. no. 113131.
[19] M. O. Williams, I. G. Kevrekidis, and C. W. Rowley, "A datadriven approximation of the Koopman operator: Extending dynamic mode decomposition," *J. Nonlinear Sci.*, vol. 25, no. 6, pp. 1307–1346, 2015.
[20] A. H. Sayed and T. Kailath, "Recursive least-squares adaptive filters," in *Digital Signal Processing Fundamentals*. Boca Raton, FL, USA: CRC Press, 2017, pp. 527–566.
[21] S. Pachnicke, *Fiber-Optic Transmission Networks*. Berlin, Germany: Springer, 2012.
[22] M. Brehler, C. Mahnke, S. Chimmalgi, and S. Wahls, "NFDM-Lab: Simulating nonlinear frequency division multiplexing in Python," in *Proc. 2019 Opt. Fiber Commun. Conf. Exhib.*, 2019, pp. 1–3.
[23] S. Klus, F. Nüske, S. Peitz, J.-H. Niemann, C. Clementi, and C. Schütte, "Data-driven approximation of the Koopman generator: Model reduction, system identification, and control," *Physica D, Nonlinear Phenomena*, vol. 406, May 2020, Art. no. 132416.